Reduced-order modeling of MEMS

Ali H. Nayfeh[a,*] Mohammad I. Younis[b], Eihab M. Abdel-Rahman[a]

[a]Department of Engineering Science and Mechanics, MC 0219, Virginia Polytechnic Institute and State University, Blacksburg, VA 24061, USA

[b]Mechanical Engineering Department, State University of New York at Binghamton, Binghamton, NY 13902, USA

Abstract

We develop reduced-order models for microelectromechanical systems (MEMS) devices using the Galerkin procedure employing the mode shapes of their structural elements. The result is a finite set of nonlinear coupled ordinary-differential equations. These equations, in turn, are used to calculate the equilibrium configurations as well as the dynamics of the devices. We apply this methodology to MEMS made of microbeams and rectangular and circular microplates. We validate these models with available experimental results and numerical solutions of the full governing partial-differential equations and associated boundary conditions.

Keywords: Reduced-order models; MEMS; Microbeams; Microplates

1. Introduction

The dynamics of microelectromechanical systems (MEMS) are represented by partial-differential equations (PDEs) and boundary conditions. Three approaches are used to reduce them to ordinary-differential equations (ODEs) in time:

- Idealization of the device flexible structural elements as rigid bodies.
- Discretization using finite-element methods (FEM), boundary-element methods (BEM), or finite-difference methods (FDM).
- Construction of reduced-order models (ROM).

The first and second approaches, while lying at opposite extremes of complexity, are currently the most widely used. The pressure for better designs, less trial-and-error in the design process, and better device performance demand better models than idealized rigid bodies. Numerous researchers compared the pull-in voltage of electrostatically actuated cantilever [1] and clamped-clamped [2] microbeams obtained by solving the distributed-parameter system to those obtained using a spring-mass model and found that the spring-mass model under-predicts the pull-in voltage.

Although FEM/BEM and FDM simulations are adequate for the analysis of the static deflections (equilibrium positions) of MEMS devices, they are inadequate for dynamic simulations because they require the time integration of thousands of second-order ODEs (one for each degree of freedom in the model). This is a very expensive process, making system-level simulation, device optimization, interactive design, and evolutionary design almost impossible. As a result, reduced-order modeling of MEMS is gaining attention as a way to balance the need for enough fidelity in the model against the numerical efficiency necessary to make the model of practical use in MEMS design.

One approach to reduced-order modeling is to eliminate the spatial dependence in the PDEs using the Galerkin method. The displacement is expressed as a linear combination of the mode-shapes (and associated eigenfunctions) $\phi_i(x,y,z)$ of the MEMS structural elements in the form:

$$w(x,y,z,t) = \sum_{i=1}^{\infty} u_i(t)\phi_i(x,y,z) \tag{1}$$

where $u_i(t)$ is the generalized coordinate associated with basis eigenfunction $\phi_i(x,y,z)$. Substituting Eq. (1) into the PDEs and requiring the residue to be orthogonal to every eigen function, we obtain an infinite set of nonlinear second-order ODEs in time in terms of the generalized coordinates $u_i(t)$. These equations are truncated to a finite set.

Next, we present reduced-order models for electrically

* Corresponding author: Tel.: +1 (540) 231 5453; Fax: +1 (540) 231 2290; E-mail: anayfeh@vt.edu

Computational Fluid and Solid Mechanics 2005
K.J. Bathe (Editor)

actuated microbeams and rectangular and circular microplates using the linear undamped mode shapes of the flat structure as a basis set in the Galerkin procedure. We also present results showing the efficiency and accuracy of these models.

2. Microbeams

We consider a clamped-clamped microbeam subject to viscous damping with a coefficient $\hat{c}$ per unit length and actuated by an electric load $v(\hat{t}) = V_{DC} + V_{AC}\cos(\Omega\hat{t})$, where V_{DC} is the DC voltage and V_{AC} and Ω are the amplitude and frequency of the AC voltage. The nondimensional equation of motion and the boundary conditions that govern the transverse deflection of the microbeam are written as [3,4]

$$\frac{\partial^4 w}{\partial x^4}+\frac{\partial^2 w}{\partial t^2}+c\frac{\partial w}{\partial t}=\left[\alpha_1\int_0^1\left(\frac{\partial w}{\partial x}\right)^2 dx+N\right]\frac{\partial^2 w}{\partial x^2}+\frac{\alpha_2 v(t)^2}{(1-w)^2} \tag{2}$$

$$w(0,t)=w(1,t)=0,\quad \frac{\partial w}{\partial x}(0,t)=\frac{\partial w}{\partial x}(1,t)=0 \tag{3}$$

where x, t, and w, are the nondimensional position, time, and transverse deflection, respectively. They are related to the dimensional variables (denoted by hats) by:

$$w=\frac{\hat{w}}{d},\quad x=\frac{\hat{x}}{\ell},\quad t=\frac{\hat{t}}{T} \tag{4}$$

where d is the capacitor gap width, ℓ is the length of the beam, and $\mathrm{T}=\sqrt{\frac{\rho A\ell^4}{EI}}$. The parameters appearing in Eq. (5) are:

$$\alpha_1=6\left(\frac{d}{h}\right)^2,\quad \alpha_2=\frac{6\epsilon\ell^4}{Eh^3d^3},\quad c=\frac{\hat{c}\ell^4}{EIT},\quad N=\frac{\hat{N}\ell^2}{EI} \tag{5}$$

where A and I are the area and moment of inertia of the cross-section, ρ is the material density, E is Young's modulus, h is the microbeam thickness, ϵ is the dielectric constant of the gap medium, and $\hat{\mathrm{N}}$ is an applied tensile axial force.

We generate a ROM [5,6] by discretizing Eqs. (2) and (3) into a finite-degree-of-freedom system consisting of ordinary-differential equations in time. We use the linear undamped mode shapes of the straight microbeam ($V_{DC} = 0$) as basis functions in the Galerkin procedure. To this end, we express the deflection as:

$$w(x,t)=\sum_{i=1}^{M}u_i(t)\phi_i(x) \tag{6}$$

We multiply Eq. (2) by $(1-w)^2$, substitute Eq. (6) into the resulting equation, use the linear undamped mode shape equation [5,6] to eliminate ϕ_n^{iv}, multiply by $\phi_n(x)$, integrate the outcome from $x = 0$ to 1, and obtain:

$$\begin{aligned}
&\ddot{u}_n-2\sum_{i,j=1}^{M}\Gamma_{ijn}\ddot{u}_i u_j+\sum_{i,j,k=1}^{M}\Gamma_{ijkn}\ddot{u}_i u_j u k_k+c\dot{u}_n-w_n^2u_n\\
&=\alpha_2\Gamma_n v(t)^2+2\sum_{i,j=1}^{M}\omega_i^2\Gamma_{ijn}u_iu_j-\sum_{i,j,k,s=1}^{M}w_1^2\Gamma_{ijkn}u_iu_ju_k\\
&+2\sum_{i,j=1}^{M}c\Gamma_{ijn}\dot{u}_iu_j-\sum_{i,j,k=1}^{M}c\Gamma_{ijkn}\dot{u}_iu_ju_k\\
&+a_1\sum_{i,j,k=1}^{M}u_iu_ju_k\int_0^1\phi_i'\phi_j'dx\int_0^1\phi_n\phi_k''dx\\
&-2\alpha_1\sum_{i,j,k,l=1}^{M}u_iu_ju_ku_l\int_0^1\phi_i'\phi_j'dx\int_0^1\phi_k\phi_l''\phi_ndx\\
&+a_1\sum_{i,j,k,l,m=1}^{M}u_iu_ju_ku_lu_m\int_0^1\phi_i'\phi_j'dx\int_0^1\phi_k''\phi_l\phi_m\phi_ndx\\
&\text{for } n=1,2,\ldots,M
\end{aligned} \tag{7}$$

where the prime denotes differentiation with respect to space x, the overdot denotes differentiation with respect to time t, ω_i, is the ith natural frequency, and the functional Γ_{ijn} is defined by:

$$\Gamma_{ijn}=\int_0^1\phi_i\phi_j\phi_ndx$$

Eq. (7) represent a discretized system of M coupled nonlinear ODEs describing the dynamic behavior of an electrically actuated microbeam. Using three or more modes in Eq. (7) was shown [5,6] to give good convergence for the stable equilibria.

When the microbeam is deflected, the linear mode shapes and natural frequencies change correspondingly. We use the ROM to calculate the fundamental natural frequency of a resonant microsensor as the voltage is increased. For a given voltage v, we substitute the static solution (fixed points of Eq. (7)) into the Jacobian matrix of Eq. (7) and find the corresponding eigenvalues. Then by taking the square root of the magnitudes of the individual eigenvalues, we obtain the natural frequencies of the microbeam. In Fig. 1 we compare the normalized fundamental natural frequency calculated using the ROM employing five symmetric modes in the discretization (solid line) with results obtained by solving the eigenvalue problem of the distributed-parameter system (triangles) using a numerical method [3,4] and the experimental results (circles) obtained by Tilmans and Legtenberg [7] for a resonator with the specifications $l = 210\,\mu\mathrm{m}$, $h = 1.5\,\mu\mathrm{m}$, $b = 100\,\mu\mathrm{m}$, $d =$

1.18 μm, E = 166 GPa, and $\hat{N}$ = 0.0009 Newtons. There is an excellent agreement among the results. The ROM shows robustness in predicting the natural frequency over the whole range of operation even as the microbeam approaches its stability limit (pull-in) where the frequency approaches zero.

To demonstrate the ROM ability to predict the dynamic behavior of microbeam-based MEMS, we calculate the pull-in time of a pressure sensor. We use the first five symmetric modes in Eq. (7) and integrate the resulting five ODEs in time for the $u_i(t)$. We find the pull-in time by monitoring the beam response over time for a sudden rise in the displacement, at that point we report the time as the pull-in time. Figure 2 shows the evolution of u_1, the dominant generalized coordinate, with the nondimensional time obtained by integrating Eq. (7). The nondimensional pull-in time is approximately t = 3.4, where a sudden rise in u_1 occurs.

3. Rectangular microplates

We model a microplate fully clamped above a parallel electrode using the dynamic analog of the von Kármán equations to account for moderately large deflections [8,9,10]. In nondimensional form, the governing equations are:

$$\frac{1}{2}(1-\nu)\left(\frac{\partial^2 u}{\partial y^2}+\alpha\frac{\partial^2 \nu}{\partial x\partial y}\right)+\frac{1}{2}(1-\nu)\left(\frac{\partial w\partial^2 w}{\partial x\partial y^2}+\frac{\partial w}{\partial y\partial x\partial y}\right)+\alpha^2\frac{\partial^2 u}{\partial x^2}+\nu\alpha\frac{\partial^2 v}{\partial x\partial y}+\alpha^2\frac{\partial w\partial^2 w}{\partial x\partial x^2}+\nu\frac{\partial w}{dy}\frac{\partial^2 w}{\partial x\partial y}=0 \tag{8}$$

$$\frac{1}{2}(1-\nu)\left(\alpha\frac{\partial^2 u}{\partial x\partial y}+\alpha^2\frac{\partial^2 \nu}{\partial x^2}\right)+\frac{1}{2}(1-\nu)\left(\alpha\frac{\partial w}{\partial x}\frac{\partial^2 w}{\partial x\partial y}+\alpha\frac{\partial w}{dy}\frac{\partial^2 w}{\partial x^2}\right)+\frac{\partial^2 u}{\partial y^2}+\nu\alpha\frac{\partial^2 u}{\partial x\partial y}+\frac{1}{\alpha}\frac{\partial w}{\partial y}\frac{\partial^2 w}{\partial y^2}+\nu\alpha\frac{\partial w}{dx}\frac{\partial^2 w}{\partial x\partial y}=0 \tag{9}$$

$$\frac{\partial^4 w}{\partial x^4}+\frac{2}{\alpha^2}\frac{\partial^4 w}{\partial x^2 dy^2}+\frac{1}{\alpha^4}\frac{\partial^4 w}{dy^4}+\frac{\partial^2 w}{\partial t^2}+\alpha_2\frac{v(t)^2}{(1-w)^2}=3\alpha_0^2\left(N_{xx}\frac{\partial^2 w}{\partial x^2}+\frac{2}{\alpha}N_{xy}\frac{\partial^2 w}{\partial x\partial y}+\frac{1}{\alpha^2}N_{yy}\frac{\partial^2 w}{\partial y^2}\right)+12\alpha_1^2\left(\frac{\partial u}{\partial x}+\nu\frac{1}{\alpha}\frac{\partial v}{\partial y}\right)\frac{\partial^2 w}{\partial x^2}+\frac{12\alpha_1^2}{\alpha^2}\left(\nu\frac{\partial u}{\partial x}+\frac{1}{\alpha}\frac{\partial v}{\partial y}\right)\frac{\partial^2 w}{\partial y^2}+12\alpha_1^2(1-\nu)\left(\frac{1}{\alpha^2}\frac{\partial u}{\partial y}+\frac{1}{\alpha}\frac{\partial v}{\partial x}\right)\frac{\partial^2 w}{\partial x\partial y}$$

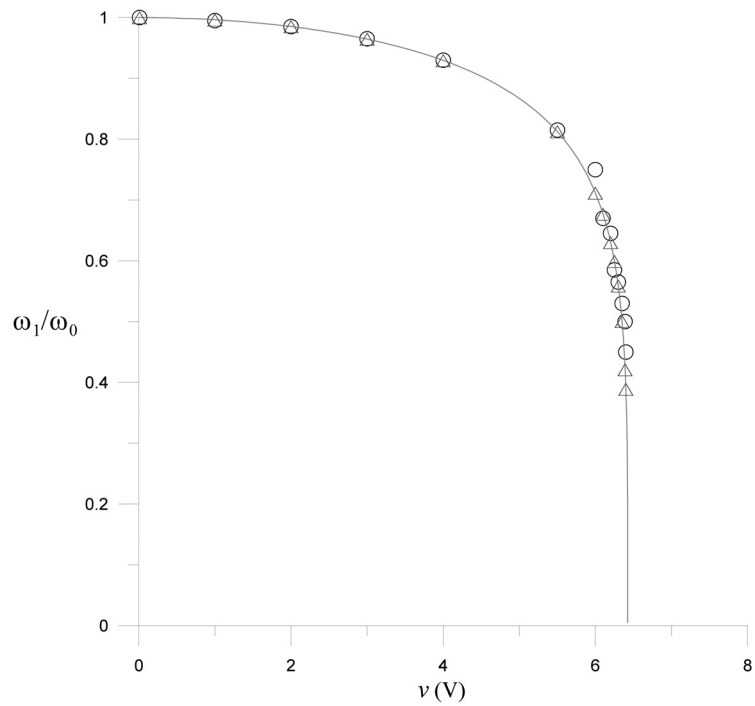

Fig. 1. A comparison of the normalized fundamental natural frequency calculated using the ROM and employing five symmetric modes in the discretization (solid line) with results obtained by Nayfeh and co-workers [3,4] (triangles) and the experimental results (circles) obtained by Tilmans and Legtenberg [7].

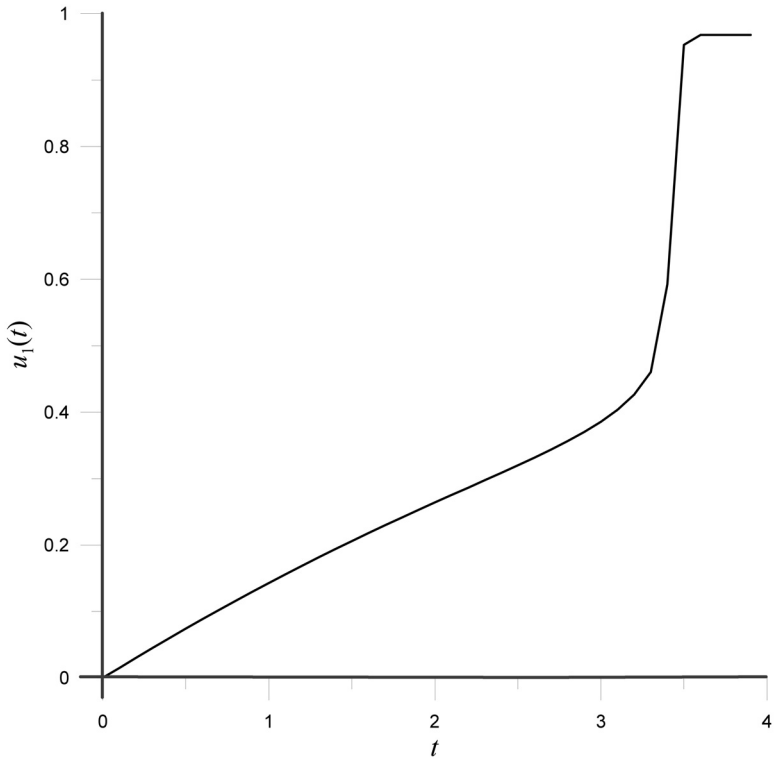

Fig. 2. Evolution of u_1 with the nondimensional time demonstrating the onset of pull-in.

$$+\frac{12\alpha_1^2}{\alpha^2}(1-\nu)\frac{\partial w}{\partial x}\frac{\partial w}{\partial y}\frac{\partial^2 w}{\partial x\partial y}$$
$$+6\alpha_1^2\left(\left(\frac{\partial w}{\partial x}\right)^2+\frac{\nu}{\alpha^2}\left(\frac{\partial w}{\partial y}\right)^2\right)\frac{\partial^2 w}{\partial x^2}$$
$$+\frac{6\alpha_1^2}{\alpha^2}\left(\frac{1}{\alpha^2}\left(\frac{\partial w}{\partial y}\right)^2+\nu\left(\frac{\partial w}{\partial x}\right)^2\right)\frac{\partial^2 w}{\partial y^2} \tag{10}$$

where $u(x,y,t)$, $v(x,y,t)$, and $w(x,y,t)$ are the displacements in the x, y, and z directions, N_{ij} is the applied force on the i-edge in the j-direction, and ν is Poisson's ratio. The nondimensional variables used in Eqs. (8)–(10) are [11]:

$$u=\frac{a\hat{u}}{2d^2},\quad v=\frac{a\hat{v}}{2d^2},\quad w=\frac{\hat{w}}{d},\quad N_{ij}=\frac{\hat{N}_{ij}}{Eh},\quad x=\frac{2\hat{x}}{a}-1,$$
$$y=\frac{2\hat{y}}{b}-1,\quad t=\frac{2h\hat{t}}{\sqrt{3(1-\nu^2)\rho a^4/E}} \tag{11}$$

This choice of x and y shifts the center of the plate to the point ($x = 0$, $y = 0$). The parameters appearing in Eqs. (8)–(10) are:

$$\alpha=\frac{b}{a},\quad \alpha_0=\frac{a}{h},\quad a_1=\frac{d}{h},\quad \alpha_2=\frac{3}{8}\frac{1-\nu^2}{Eh^3d^3}\epsilon a^4 \tag{12}$$

Zhao et al. [11] solved the linear undamped eigenvalue problem using the hierarchical finite-element method (HFEM) to obtain the microplate eigenfunctions $\phi_i(x, y)$ and write the transverse displacement field as:

$$w(x,y,t)=\sum_{i=1}^{M} q_i(t)\phi_i(x,y) \tag{13}$$

Substituting Eq. (13) into Eqs. (8) and (9) and considering the associated in-plane boundary conditions yields a set of boundary-value problems for u and v. Using the HFEM, Zhao et al. [11] solved for u and v in terms of $q_i(t)$; that is:

$$u=u(x,y,q_i(t))\quad\text{and}\quad v=v(x,y,q_i(t)) \tag{14}$$

Multiplying both sides of Eq. (10) by $(1 - w)^2$, substituting Eqs. (13) and (14) into the outcome, and applying the Galerkin procedure, we obtain a set of nonlinearly coupled ODEs, which is the ROM for the microplate.

Francais and Dufour [12] measured the center deflection of a fully clamped square microplate under various electrostatic actuations. In Fig. 3, we compare the deflection w_{max} at the center of the plate calculated using the ROM with the experimental results of

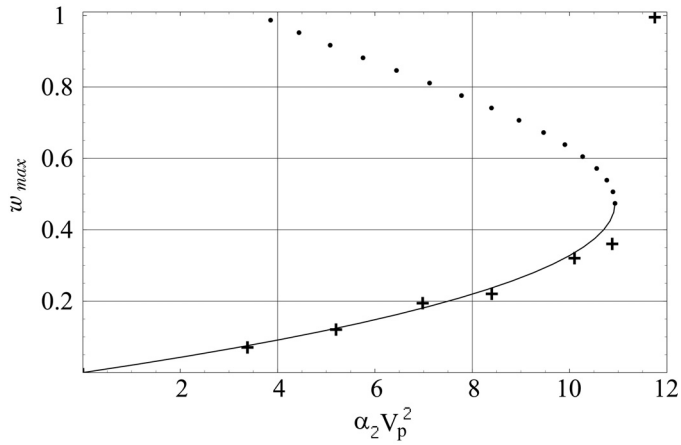

Fig. 3. Comparison of w_{max} calculated using the ROM (solid and dotted curves) with the experimental results (+) of Francais and Dufour [12].

Francais and Dufour. The ROM shows good agreement and robustness, being able to predict deflections up to the pull-in voltage. The dots correspond to unstable equilibrium solutions and the solid line corresponds to stable equilibrium solutions calculated using the ROM.

4. Circular microplates

We consider a circular plate with radius R fully clamped above a parallel electrode. The nondimensional equations governing the axisymmetric deflection $w(r,t)$ of the plate can be written as [13]:

$$\frac{\partial^2 w}{\partial t^2}+\nabla^4 w=\beta\left[\frac{1}{r}\frac{\partial}{\partial r}\left(\frac{\partial w}{\partial r}\frac{\partial \Phi}{\partial r}\right)+\frac{\sigma}{r}\frac{\partial}{\partial r}\left(r\frac{\partial w}{\partial t}\right)-2c\frac{\partial w}{\partial t}+F(r,t)\right]+\frac{\upsilon(t)^2}{(w_{max}-w)^2} \tag{15}$$

$$\nabla^4\Phi=-\frac{1}{r}\frac{\partial^2 w}{\partial r^2}\frac{\partial w}{\partial r} \tag{16}$$

where ∇^4 is the polar biharmonic operator, σ is the residual stress, $F(r,t)$ is an additional axisymmetric pressure, and $\Phi(r,t)$ is the stress function. The nondimensional variables and parameters appearing in Eqs. (15) and (16) are given by:

$$w=\frac{R}{h^2}\hat{w},\quad w_{max}=\frac{R}{h^2}d,\quad r=\frac{\hat{r}}{R},\quad t=\sqrt{\frac{D}{\rho h}}\frac{\hat{t}}{R^2},$$

$$F=\frac{R^7\hat{F}}{12(1-\nu^2)Dh^4},\quad \upsilon(t)^2=\frac{\epsilon R^7\hat{\upsilon}(t)^2}{2Dh^2},$$

$$\sigma=\frac{R^4\hat{\sigma}}{Eh^4},\quad \Phi=\frac{R^2\hat{\Phi}}{Eh^5}, \tag{17}$$

$$c=\frac{R^4}{24(1-\nu^2)}\frac{\hat{c}}{\sqrt{\rho h^5 D}},\quad \text{and } \beta=\frac{12(1-\nu^2)h^2}{R^2}$$

and $D=\frac{Eh^2}{12(1-\nu^2)}$ is the plate flexural rigidity. The boundary conditions are:

$$w(1,t)=0,\quad \frac{\partial w(1,t)}{\partial r}=0,\quad \text{and } w\ (0,t);\ \text{is bounded} \tag{18}$$

To generate the ROM, we let:

$$w(r,t)=\sum_{m=1}^{M}\eta_m(t)\phi_m(r) \tag{19}$$

$$\Phi(r,t)=\sum_{m,n=1}^{M}\eta_m(t)\eta_n(t)\psi_{mn}(r) \tag{20}$$

where $\phi_m\ (r)$ is the mth axisymmetric linear undamped mode shape of the flat plate ($\beta=0$) and the $\Psi_{mn}\ (r)$ are unknown axisymmetric functions to be determined in the course of the analysis. Substituting Eqs. (19) and (20) into Eqs. (15), (16), and (18), and following the Galerkin procedure, we obtain:

$$w_{max}^2\left(\ddot{\eta}_q+2c\dot{\eta}_q+\omega_q^2\eta_q\right)-2w_{max}\sum_{i,j=1}^{M}\Gamma_{ijq}\left(\ddot{\eta}_j+2c\dot{\eta}_j+\omega_j^2\eta_j\right)\eta_i+\sum_{i,j,k=1}^{M}\Gamma_{ijkq}\left(\ddot{\eta}_k+2c\dot{\eta}_k+\omega_k^2\eta_k\right)\eta_i\eta_j$$
$$=\Gamma_q\upsilon^2(t)+\beta\left[-\omega_{max}^2\sum_{i,j,k=1}^{M}\eta_i\eta_j\eta_k\int_0^1\phi_q'\phi_i'\psi_{jk}'dr\right.$$

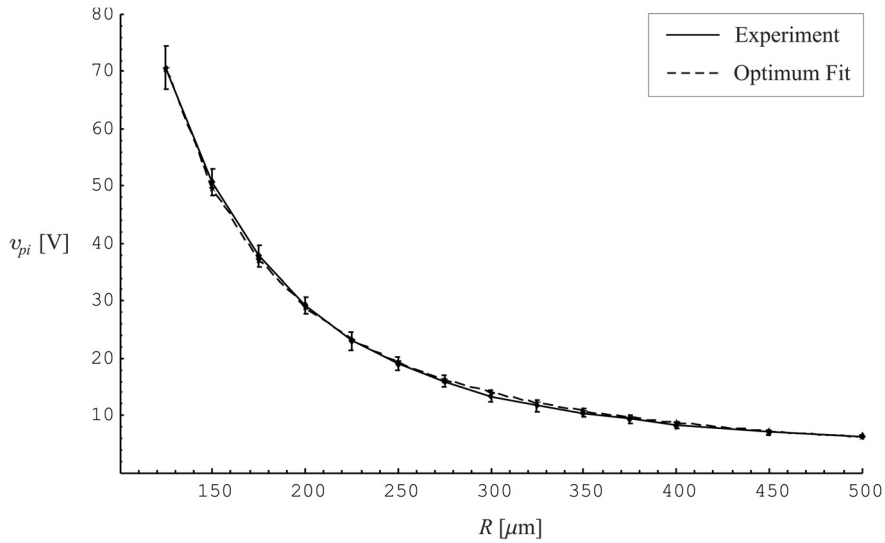

Fig. 4. Comparison of the pull-in voltage variation with plate radius obtained using the ROM and the experimental results of Osterberg [14].

$$+2\omega_{max}\sum_{i,j,k,l=1}^{M}\eta_i\eta_j\eta_k\eta_l\int_0^1(\phi_1\phi_q)'\phi_j'\psi_{kl}'dr$$

$$-\sum_{i,j,k,l,m=1}^{M}\eta_i\eta_j\eta_k\eta_l\eta_m\int_0^1(\phi_i\phi_j\phi_q)'\phi_k'\psi_{lm}'dr$$

$$-\sigma\omega_{max}^2\sum_{m=1}^{M}\eta_i\int_0^1 r\phi_i'\phi_q'dr$$

$$+2\sigma\omega_{max}\sum_{i,j=1}^{M}\eta_i\eta_j\int_0^1 r\phi_j'(\phi_i\phi_q)'dr$$

$$-\sigma\sum_{i,j,k=1}^{M}\eta_i\eta_j\eta_k\int_0^1 r\phi_k'(\phi_i\phi_j\phi_q)'dr+\omega_{max}^2\int_0^1 Fr\phi_q dr$$

$$-2\omega_{max}\sum_{i=1}^{M}\eta_i\int_0^1 Fr\phi_i\phi_q dr+\sum_{i,j=1}^{M}\eta_i\eta_j\int_0^1 Fr\phi_i\phi_j\phi_q dr\Bigg]$$

$$q=1,\ \ldots,\ M \tag{21}$$

$$\psi_{ij}'(r)=-\frac{r}{4}\int_0^r\frac{\phi_i'\phi_j'}{\xi}d\xi+\frac{1}{4r}\int_0^r\xi\phi_i'\phi_j'd\xi+\frac{r}{4}\int_0^1\frac{\phi_i'\phi_j'}{\xi}d\xi$$

$$+\frac{r}{4}\frac{1+\nu}{1+\nu}\int_0^1\xi\phi_i'\phi_j'd\xi\quad i,j=1,\ldots,M \tag{22}$$

where the functional Γ_{ijn} is defined as:

$$\Gamma_{ijq}=\int_0^1\phi_i\phi_j\phi_q dx$$

Vogl and Nayfeh [13] validated the ROM with experimental data. Osterberg [14] measured the pull-in voltage v_{pi} for multiple radii R of clamped circular microplates made of silicon with the specifications $h\approx 3\,\mu$m and $d\approx 1\,\mu$m. Osterberg developed a statistics-based model to approximate v_{pi} and solved for the optimal statistical coefficients by fitting his model to the experimental data. Vogl and Nayfeh [13] fit the physics-based model, Eqs. (21) and (22), to the experimental data by solving for the values of E, σ, ν, d, and h that minimize the objective function:

$$W=\sum_{i=1}^{14}\left(\frac{v_i^{model}(E,\sigma,\nu,d,h)-v_i^{exp}}{\delta_i}\right)^2 \tag{23}$$

where the δ_i, v_i^{model}, and v_i^{exp} are, respectively, the experimental standard deviations, the model pull-in values, and the experimental pull-in values for the 14 different experimental radii. The objective function W is a weighted sum of the square of the deviations between the model and experimental values. The local minimum of W is $d=1.014\,\mu$m, $h=3.01\,\mu$m, $E=150.6$ GPa, $\nu=0.0436$, and $\hat{\sigma}=7.82$ MPa, which seems to be the global minimum. The pull-in voltages from this optimum model are displayed in Fig. 4 along with the experimental data. Standard deviation bars for the experimental data are also shown in the figure.

5. Summary and conclusions

We used the mode shapes of the structural elements of MEMS devices as basis sets in the Galerkin procedure to develop ROMs for microbeams and rectangular and circular microplates and validated them with

experimental and full numerical solutions. Our approach to the construction of ROMs has proven to be robust and accurate over the whole operation range of the device, including pull-in. These ROMs need to be extended to a broader class of devices, employing more complex structural elements.

References

[1] Zavracky PM, Majumder S, McGruer NE. Micromechanical switches fabricated using nickel surface micromachining. Journal of Microelectromechanical Systems 1997;6:3–9.

[2] Choi B, Lovell EG. Improved analysis of microbeams under mechanical and electrostatic loads. Journal of Microelectromechanical Systems 1997;7:24–9.

[3] Abdel-Rahman EM, Younis MI, Nayfeh, AH. Characterization of the mechanical behavior of an electrostatically actuated microbeam. Journal of Micromechanics and Microengineering 2002;12:759–766.

[4] Younis MI, Abdel-Rahman EM, Nayfeh, AH. Static and dynamic behavior of an electrically excited resonant microbeam. Proc of the 43rd AIAA Structures, Structural Dynamics, and Materials Conference, Denver, CO, 2002.

[5] Abdel-Rahman EM, Younis MI, Nayfeh, AH. A nonlinear reduced-order model for electrostatic MEMS. Proceedings of ASME Design Engineering Technical Conferences, DETC'03, Chicago, IL, 2003.

[6] Younis MI, Abdel-Rahman EM, Nayfeh, AH. A reduced-order model for electrically actuated microbeam-based MEMS. Journal of Microelectromechanical Systems 2003;12:672–680.

[7] Tilmans HA, Legtenberg R. Electrostatically driven vacuum-encapsulated polysilicon resonators. Part II: Theory and performance. Sensors and Actuators A 1994;45:67–84.

[8] Nayfeh AH, Mook DT. Nonlinear Oscillations. New York: Wiley, 1979.

[9] Nayfeh AH. Nonlinear interactions. New York: Wiley, 2000.

[10] Nayfeh AH, Pai FP. Linear and nonlinear structural mechanics. New York: Wiley, 2004.

[11] Zhao X, Abdel-Rahman EM, Nayfeh AH. Mechanical behavior of an electrically actuated microplate. Proc of ASME Design Engineering Technical Conferences, DETC'03, Chicago, IL, 2003.

[12] Francais O, Dufour I. Normalized abacus for the global behavior of diaphragms: pneumatic, electrostatic, piezoelectric or electromagnetic actuation. Journal of Modeling and Simulation of Microsystems 1999;2:149–160.

[13] Vogl GW, Nayfeh AH. A reduced-order model for electrically actuated clamped circular plates. Proc of ASME Design Engineering Technical Conference, DETC'03, Chicago, IL, 2003.

[14] Osterberg P. Electrostatically actuated microelectromechanical test structures for material property measurement, PhD Dissertation, Massachusetts Institute Technology, 1995.